

Beach Profile Equilibrium and Patterns of Wave Decay and Energy Dissipation across the Surf Zone Elucidated in a Large-Scale Laboratory Experiment

Ping Wang[†] and Nicholas C. Kraus[‡]

[†]Department of Geology
University of South Florida
4202 E. Fowler Ave.
Tampa, FL 33620, U.S.A.
pwang@chuma1.cas.usf.edu

[‡]U.S. Army Engineer
Research and Development
Center
Coastal and Hydraulics
Laboratory
3909 Halls Ferry Road
Vicksburg, MS 39180, U.S.A.

ABSTRACT

WANG, P. and KRAUS, N.C., 2005. Beach profile equilibrium and patterns of wave decay and energy dissipation across the surf zone elucidated in a large-scale laboratory experiment. *Journal of Coastal Research*, 21(3), 522-534. West Palm Beach (Florida), ISSN 0749-0208.



The widely accepted assumption that the equilibrium beach profile in the surf zone corresponds with uniform wave-energy dissipation per unit volume is directly examined in six cases from the large-scale SUPERTANK laboratory experiment. Under irregular waves, the pattern of wave-energy dissipation across a large portion of the surf zone became relatively uniform as the beach profile evolved toward equilibrium. Rates of wave-energy dissipation across a near-equilibrium profile calculated from wave decay in the surf zone support the prediction derived by DEAN (1977). Substantially different equilibrium beach-profile shapes and wave-energy dissipation rates and patterns were generated for regular waves as compared to irregular waves of similar statistical significant wave height and spectral peak period. Large deviation of wave-energy dissipation from the equilibrium rate occurred at areas on the beach profile with active net cross-shore sediment transport and substantial sedimentation and erosion. The rate of wave-energy dissipation was greater at the main breaker line and in the swash zone, as compared to middle of the surf zone. Based on analysis of the SUPERTANK data, a simple equation is developed for predicting the height of irregular waves in the surf zone on an equilibrium profile. The decay in wave height is proportional to the water depth to the one-half power, as opposed to values of unity or greater derived previously for regular waves.

ADDITIONAL INDEX WORDS: *Beach profile, equilibrium, cross-shore sediment transport, wave breaking, coastal morphology, SUPERTANK, physical modeling.*

INTRODUCTION

The concept of an equilibrium shape of the beach profile has proved fruitful in a variety of applications in coastal science and engineering, such as beach nourishment design and studies concerned with morphological evolution in the near-shore. Under this concept, if the incident waves and water level remain constant, the beach profile is expected to evolve toward a stable shape for which the net cross-shore sediment transport rate across the profile approaches zero. Assumptions underlying the simplest such situation involving analytical solutions are alongshore uniformity, uniform or nearly uniform sized sediment, absence of obstructions such as hard bottom on the beach profile, and dominance of wave action as the driving process shaping the profile. These assumptions can be relaxed in numerical solutions, such as that of LARSON and KRAUS (2000) for describing profile evolution in the presence of hard bottom. In the study described here, we investigate the equilibrium profile shape in response to breaking waves, *i.e.*, the profile shape in the surf zone on sandy beach-

es. INMAN *et al.* (1993) discussed equilibrium profile shapes inside and outside the surf zone, with the offshore bar acting as a hinge point.

In a pioneering study of the beach profile, BRUUN (1954) noted that the shape of the nearshore beach profile along the coast of Denmark followed a simple power law of depth with distance seaward from the shoreline. In a macro-scale approach depending on general characteristics of the incident waves and representative beach material grain size, DEAN (1977) derived classes of beach profile shapes that depend on choice of the governing mechanism assumed to control the transport processes. The choice that best corresponded to field data for Atlantic Ocean and Gulf of Mexico beaches yielded a shape similar to that found by BRUUN (1954) in a derivation for which the wave-energy-flux dissipation per unit water volume is uniform. The result of DEAN (1977) has led to a standard equilibrium beach profile shape given by:

$$h = A_x^{2/3} \quad (1)$$

where h is the still-water depth, x is the horizontal distance from shoreline ($h = 0$), and A is a dimensional scale parameter having units of $m^{1/3}$ and a value determined mainly by

sediment grain size (DEAN, 1977; MOORE, 1982; DEAN, 1991; MOUTZOURIS, 1991).

Many studies have shown that Equation (1) or a similar form represents the time- and locally-averaged shape of the beach profile with ample sediment supply on a coast exposed to waves and uninfluenced by structures and hard bottom (e.g., MOORE, 1982; LARSON, 1991; WORK and DEAN, 1991; PRUSZAK, 1993; LARSON and KRAUS, 1994a; WANG and DAVIS, 1998, 1999; LARSON *et al.*, 1999; GONZALEZ *et al.*, 1999). LARSON and KRAUS (1989) derived an analytical form for the beach profile shape at equilibrium under the realistic wave decay model of DALLY *et al.* (1985) that has a planar shape at the foreshore joining to the form of Equation (1) further in the surf zone. LARSON *et al.* (1999) derived the power-function beach profile (Eq. 1) from a non-local balance of time-averaged offshore and onshore sediment transport. These and other studies give confidence that Equation (1) both describes nature and has a consistent theoretical basis. However, to our knowledge, no equilibrium mechanism has been directly tested by comparisons to laboratory or field measurements of wave dissipation and grain size. Hereafter, this paper considers wave-energy dissipation per unit volume in the surf zone and its relation to the equilibrium profile.

In the DEAN (1977) derivation of Equation (1) based on uniform dissipation of wave-energy flux per unit volume across the surf-zone profile, the spilling breaking wave assumption was invoked, meaning the height H of broken waves in the surf zone is proportional to the depth h . The equilibrium wave-energy dissipation D_* across the surf zone is then (DEAN, 1977):

$$D_* = \frac{5}{24} \gamma^2 \rho_w g^{3/2} A^{3/2} \quad (2)$$

where ρ_w is the density of water, g is the acceleration of gravity, and γ is the breaker index for depth-limited waves, defined as wave height over water depth (H/h) for breaking or broken waves. KAMINSKY and KRAUS (1993) found that the commonly used value for incipient breaking of depth-limited individual breaking waves, $\gamma = 0.78$, is supported by a large laboratory database for regular (monochromatic) waves. They also found limits for γ in the more than 400 individual measurements to lie within 0.60 and 1.59.

For a train of waves with different heights (irregular waves), at a given location in the surf zone, the γ value for significant wave height H_s is also found to be close to 0.78. However, root-mean-square wave height H_{rms} is appropriate for calculation of mean wave energy in an irregular wave field. At a given location, this quantity has a γ (rms) value in the approximate range of 0.4 to 0.6 for irregular waves in the surf zone (e.g., THORNTON and GUZA, 1982, 1983; WANG *et al.*, 2002a, 2002b), because the ratio H/h is formed by the combination of breaking, broken, and non-breaking waves. Field measurements analyzed by THORNTON and GUZA (1982, 1983) gave a value of γ_{rms} in the range of 0.42 to 0.44.

Wave-energy-flux dissipation per unit water volume across shore $D(x)$ can be calculated from measurements of wave height and water depth at adjacent, closely spaced wave gauges as:

$$D(x) = \frac{1}{h} \frac{d(EC_g)}{dx} = \frac{1}{h} \frac{d\left(\frac{1}{8} \rho_w g H_{rms}^2 \sqrt{gh}\right)}{dx} \approx \frac{1}{8} \frac{\rho_w g^{3/2}}{h_{mid}} \frac{\Delta(H_{rms}^2 h^{1/2})}{\Delta x} \quad (3)$$

where E is the wave energy per unit area, $C_g = \sqrt{gh}$ is the wave group velocity in shallow water, and h_{mid} is the water depth at the mid-point between the wave gauges used here to approximate the energy dissipation per unit volume.

The concept of beach-profile equilibrium and the corresponding uniform wave-energy dissipation underlie a number of practical cross-shore sediment-transport and beach-profile evolution models (e.g., KRIEBEL and DEAN, 1985; KRIEBEL, 1986; LARSON and KRAUS, 1989; ZHENG and DEAN, 1997). In development of these models, it is assumed that wave-energy dissipation rates (Eq. 3) will deviate substantially from the equilibrium rate (Eq. 2) during high-wave energy storms, because the equilibrium beach profile and associated wave-energy dissipation would tend to represent the average condition of all waves, as demonstrated with high-accuracy field data (LARSON and KRAUS, 1994a). Therefore, the net cross-shore sediment transport rate q and beach-profile evolution depend on the magnitude of deviation from an equilibrium state (e.g., KRIEBEL and DEAN, 1985; KRIEBEL, 1986; KRAUS and LARSON, 1988; LARSON and KRAUS, 1989):

$$q = K(D - D_*)^n \quad (4)$$

where K and n are empirical coefficients. The original studies employing this form took $n = 1$, but larger values such as $n = 1.5$ have been advocated to increase the time rate of change at longer elapsed time (ZHENG and DEAN, 1997).

Because Equation (2) quantifies the equilibrium rate of dissipation per unit water volume in both theoretical and applied treatments of beach-profile change, it is of central interest to assess its validity under realistic conditions. The validation should answer two questions: 1) Is the wave-energy dissipation rate uniform across the equilibrium surf-zone profile as assumed, and 2) If (1) is true, how well does Equation (2) predict the magnitude of the equilibrium rate of wave-energy dissipation per unit volume?

The SUPERTANK large-scale laboratory data collection project (KRAUS *et al.*, 1992; KRAUS and SMITH, 1994; SMITH and KRAUS, 1995) documented beach-profile response to accretionary waves, erosional waves, and different boundary conditions, together with high-density measurements of waves and currents in the surf zone. The SUPERTANK data set has enabled examination of a wide range of cross-shore processes from, for example, beach profile response to a seawall (McDOUGAL *et al.*, 1996) through detailed investigations of net cross-shore sand transport (LARSON and KRAUS, 1994b) and surf-zone hydrodynamics (KRIEBEL and SMITH, 1994; SMITH, 1994).

For the present study, profile survey data and wave measurements across the surf zone made at SUPERTANK are analyzed to test the assumptions that at or near equilibrium of the beach profile, wave-energy-flux dissipation per unit water volume is uniform across the surf zone, and with a

Table 1. SUPERTANK data used in this study.

Run ID	Duration of wave action (min)	H_{mo} before breaking (m)	T_p (s)	γ_{sw}	Comments
ST_10-1-20	20	0.8	3.0	20	initial profile
ST_10-1-270	270	0.8	3.0	20	end profile
ST_30-1-9	9	0.4	9.0	20	initial profile
ST_30-1-279	279	0.4	9.0	20	end profile
ST_10-2-5	5	0.8	4.5	3.3	initial profile
ST_10-2-170	170	0.8	4.5	3.3	end profile
ST_30-2-9	9	0.4	8.0	3.3	initial profile
ST_30-2-209	209	0.4	8.0	3.3	end profile
ST_G0-1-9	9	0.8	3.0	Mon	initial profile
ST_G0-1-210	210	0.8	3.0	Mon	end profile
ST_10-1-20	20	0.5	8.0	Mon	initial profile
ST_10-1-559	559	0.5	8.0	Mon	end profile

value close to that given by Equation (2). Six cases from the SUPERTANK dataset were selected that had constant waves run for at least 3 hours. The cases cover considerably different wave conditions. The objectives of this study are to examine (1) patterns of surf-zone-profile evolution under various wave conditions; (2) patterns of wave decay and wave-energy dissipation associated with the profile change and incident waves; (3) hypothesis that uniform wave-energy-flux dissipation per unit volume occurs over an equilibrium profile; and (4) the accuracy of Equation (2) if uniform wave-energy dissipation is achieved on a near-equilibrium beach profile. In addition, a new equation is derived that describes decay in height of irregular waves on an equilibrium profile.

SUPERTANK EXPERIMENTS

SUPERTANK was designed to collect data without scaling distortions to improve understanding and predictive capabilities on cross-shore sediment transport processes (KRAUS *et al.*, 1992). The experiments were conducted in the large wave channel at the O. H. Hinsdale Wave Research Laboratory at Oregon State University. The channel is 104 m long, 3.7 m wide, and 4.6 m deep, into which a 76-m long sand beach was emplaced for the SUPERTANK experiments. The flap-type wave generator was equipped with a sensor and feedback mechanism to absorb reflected waves at the peak energy. The beach was composed of approximately 600 m³ of very-well sorted fine sand with a median diameter of 0.22 mm and an average fall speed of 3.3 cm/s. Based on equations developed by MOORE (1982) and DEAN (1991), the A -value in Equation (1) corresponding to this grain size is 0.10 m^{1/3}. A larger A -value of 0.17 m^{1/3} was specified in the initial beach construction to create a steeper profile to ensure adequate water depth in the offshore area (KRAUS and SMITH, 1994). In design of the SUPERTANK tests, erosion or accretion of the profile was predicted prior to running the waves by relations given by KRAUS *et al.* (1991) to arrange instruments, video cameras, and satisfy requirements for participating investigators.

Six cases from the SUPERTANK data set were judged suitable (with sufficient duration) for this study (Table 1). In the following discussion and figures, the run ID, *e.g.*, ST_10-1-20, indicates the following information: 1) the first five char-

acters, ST_10, denote the SUPERTANK test case, (which includes a number of wave-run segments typically with 10 to 70 min of wave action each); 2) the next two characters, -1, indicate a selected block in the ST_10 experiment, which is composed of several bursts or time intervals with the same input waves, and 3) the characters following the last hyphen indicate the number of minutes of the particular wave action (could be the sum of several wave-run segments, particularly for the end profile). Still-water level in the channel was constant and the same for these tests.

Narrow-peaked (swell type) irregular waves with γ_{sw} (spectral width parameter) = 20 (BOUWS *et al.*, 1985) were generated during the first two cases, ST_10-1 and ST_30-1. Steep erosional waves with a significant wave height H_s of 0.8 m and spectral peak wave period T_p of 3 s, were generated in ST_10-1. The initial beach profile was constructed based on Equation (1) with an A -value of 0.17 m^{1/3}. The end profile resulted from a total of 270 min of wave action. Mild-steepness accretionary waves with a significant height of 0.4 m and peak period of 9 s were generated in ST_30-1. The initial profile was the final profile of a previous 130-min wave run ($H_s = 0.5$ m, $T_p = 8$ s, $\gamma_{sw} = 3.3$). The end profile of ST_30-1 was shaped by a total of 279 min of wave action.

Broad-peaked (sea type) irregular waves with $\gamma_{sw} = 3.3$ were generated during the cases, ST_10-2 and ST_30-2. Steep erosional waves with significant height of 0.8 m and peak period of 4.5 s were generated during ST_10-2. The initial profile was the final profile of a previous 280-min narrow-peaked wave run ($H_s = 0.8$ m, $T_p = 4.5$ s, $\gamma_{sw} = 20$). The end profile of ST_10-2 was shaped by a total of 170 min of wave action. Gentle accretive waves, with significant height of 0.4 m and peak period of 8 s were generated in ST_30-2. The initial profile was the final profile of a previous wave run of varying wave heights and periods. The end profile was shaped by a total of 209 min of wave action.

Regular (monochromatic) waves were generated during the last two cases of SUPERTANK, ST_G0-1 and ST_I0-1. Steep erosional waves with height of 0.8 m and period of 3 s were generated in ST_G0-1. The significant wave height and peak wave period are similar to those of ST_10-1, except the waves were monochromatic. Different energy levels are carried by regular and irregular waves with identical significant wave heights. This is because for regular waves, significant wave height equals root-mean-square (rms) wave height, which is directly proportional to wave energy, whereas for irregular waves, significant wave height equals 1.4 times the rms wave height for Rayleigh-distributed waves. The initial profile was the final profile of a previous wave run of varying wave heights and periods. The end profile of ST_G0-1 resulted from a total of 210 min of wave action. Mild-steepness accretionary waves with height of 0.5 m and period of 8 s were generated in ST_I0-1. The significant wave height and peak period are similar to those of ST_30-2, except that the waves were monochromatic. The initial profile was the final profile of a previous wave run of varying wave heights and periods. The end profile of ST_I0-1 was shaped by 559 min total wave action.

The beach profile was surveyed across the middle of the 3.66-m wide channel at the end of each wave-run segment,

typically 10 to 70 min long. A Geodimeter T140 survey station was positioned outside of the tank to track by an infrared beam the position of the prism mounted on the top of the rod. Reproducibility of the elevation measurement was typically within 0.5 cm except at the shoreward face of steep break-point bars, where the variation in reproducibility decreased to a nominal 2 cm (KRAUS *et al.*, 1992).

Waves were measured at 26 cross-shore locations by resistance gauges, spanning from the swash zone to approximately 70 m seaward of the shoreline. The wave gauges were sampled at 16 Hz. Both spectral analysis and time-series zero-upcrossing analysis were applied to calculate wave height and period (KRAUS and SMITH, 1994). A low-pass filter was applied to separate incident-band wave motion from low-frequency motions. A high-pass time series was thus obtained by subtracting the low-pass time series from the preprocessed data (KRAUS and SMITH, 1994, pp.62–66). The period cutoff for the filter was set to twice the peak period of the incident waves. This data filtering has considerable influence on the calculation of wave height and period in the swash zone, where long-period motion was significant and sometime dominant. The wave data analyzed in this paper were processed with the above data filtering and, therefore, the wave height referenced in the following analysis does not include contributions from low-frequency motions. The root-mean-square wave height and mean wave period calculated from the zero-upcrossing analysis were used to calculate wave-energy dissipation.

The rate of wave-energy-flux dissipation was calculated from the measurements at two adjacent wave gauges based on Equation (3) and is represented (plotted in the following figures) at the mid-point between them. Typically, eight wave gauges were located in the swash zone, spaced at 0.9-m interval. Two wave gauges were located seaward of the swash gauges, spaced at 1.8 m. Sixteen gauges were located through and beyond the surf zone, spaced at 3.7-m interval. Given the close spacing between the wave gauges, Equation (3) is expected to provide reliable estimates of wave-energy dissipation rate per unit water volume for the SUPERTANK wave conditions, except possibly in areas of extreme gradients in wave height, *e.g.*, in the vicinity of plunging breakers.

RESULTS

In the six cases examined and nearly all the SUPERTANK runs, a breakpoint bar, or bar in the area of incipient depth-limited wave breaking, developed on the initial monotonic power-function beach profile as described by Equation (1). Little change occurred in the offshore region outside the surf zone in the cases examined here. All profiles examined in this study are displayed in Figure 1. The surf-zone portions of the profiles are not directly comparable among different tests, particularly in the vicinity of shoreline where the beach might have been reconfigured for different objectives. However, the offshore area was not reconstructed. The following discussion pertains the beach profile at and landward of the break-point bar (the surf zone).

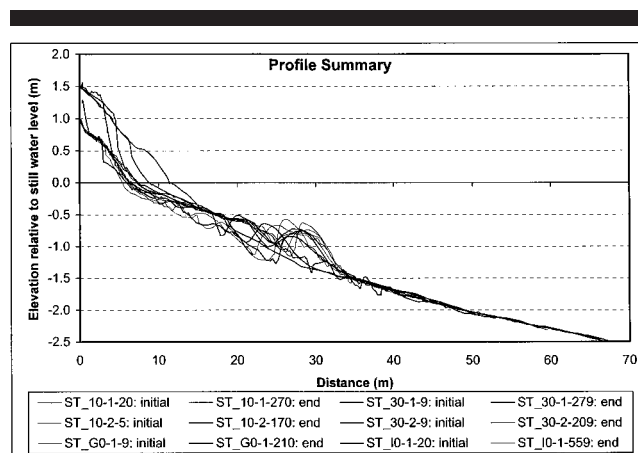


Figure 1. All beach profiles examined in this study; note that the profile changed little seaward of the bar.

Beach-Profile Evolution

Test ST-10-1 with steep, narrow-band erosional waves was the first run of SUPERTANK. The initial profile was the monotonic power-function profile constructed with $A = 0.17 \text{ m}^{1/3}$. Considerable shoreline recession of approximately 2.5 m and development of a 30-cm high break-point bar occurred (Figure 2A). The erosion in the vicinity of the shoreline roughly equaled the accumulation in the bar area, while beach elevation remained largely unchanged over a considerable area from 15 to 20 m between the swash zone and the main breaker line over the bar (Figure 2A). This morphologic change indicates that the sand eroded from the shoreline was transported offshore across an area in the mid-surf zone and deposited near the main breaker line to form the break-point bar. Moderate erosion in the trough and slight accumulation directly landward of it also occurred.

The initial surf-zone profile represents the power-function profile with $A = 0.17 \text{ m}^{1/3}$ well, as constructed. The constructed profile was slightly gentler in the inner surf zone and steeper in the outer surf zone, as compared to $A = 0.17 \text{ m}^{1/3}$ profile. After 270 min of wave action, the end surf-zone profile had a much gentler overall slope than the initial slope because of erosion in the vicinity of the original shoreline and development of the break-point bar. An equilibrium profile shape with $A = 0.17 \text{ m}^{1/3}$ over-predicts the water depth across most of the surf zone, except at the bar trough. The value $A = 0.10 \text{ m}^{1/3}$, which corresponds to the SUPERTANK grain size of 0.22 mm according to MOORE (1982) and DEAN (1991), predicts the profile shape reasonably well across most of the surf zone, except at the trough, where water depth is under-predicted considerably.

For the remainder of the three irregular wave cases (Figure 2B and Figure 3), the magnitude of the beach-profile change was much smaller as compared to the initial changes (Figure 2A), especially during the accretionary wave cases with lower waves (Figure 2B and Figure 3B). The bar became slightly wider and flatter, as compared to the initial profile after the accretionary wave actions. Considerable berm erosion above

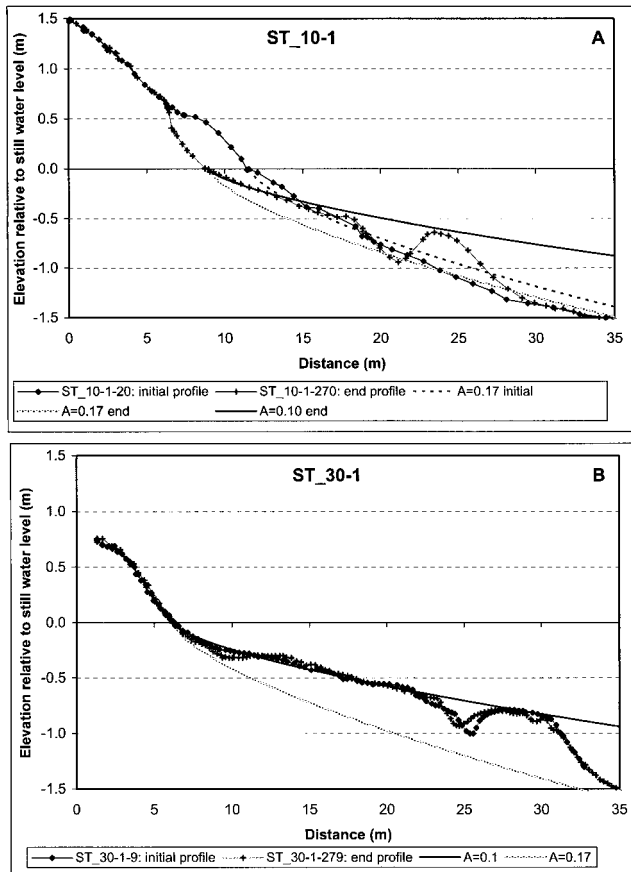


Figure 2. Initial and end beach profiles for ST.10-1 and ST.30-1, and the power-function profiles.

mean water level occurred during the steep, broadband (sea type) erosional waves (Figure 3A). The eroded sand was deposited in a relatively thin layer across the mid-surf zone extending to the bottom of the trough. The average elevation from 8 to 25m across shore gained 2.4 cm during the 170-min wave action. The elevation of the bar remained nearly stable at the beginning and end of the wave action, but moved approximately 0.5 m offshore.

Similar to ST.10-1, the surf-zone profile can be represented more accurately with $A = 0.10 \text{ m}^{1/3}$ (except at the trough), whereas $A = 0.17 \text{ m}^{1/3}$ over-predicts water depth across most of the surf zone except at the trough, especially for the accretive wave cases (Figures 2B and 3B). In other words, the initially constructed steep profile was out of equilibrium and evolved toward a gentler profile, as predicted by the DEAN (1977) profile model. The A of $0.10 \text{ m}^{1/3}$ gives an equilibrium profile shape matching the end profile well.

Considerable change between the initial and end profiles occurred during the regular wave cases (Figure 4A and B). During the erosional case with higher waves (Figure 4A), the bar moved onshore and became considerably higher after 210 min of wave action. Moderate erosion near the shoreline also occurred. No profile change occurred seaward of the bar outside the surf zone, whereas considerable changes occurred

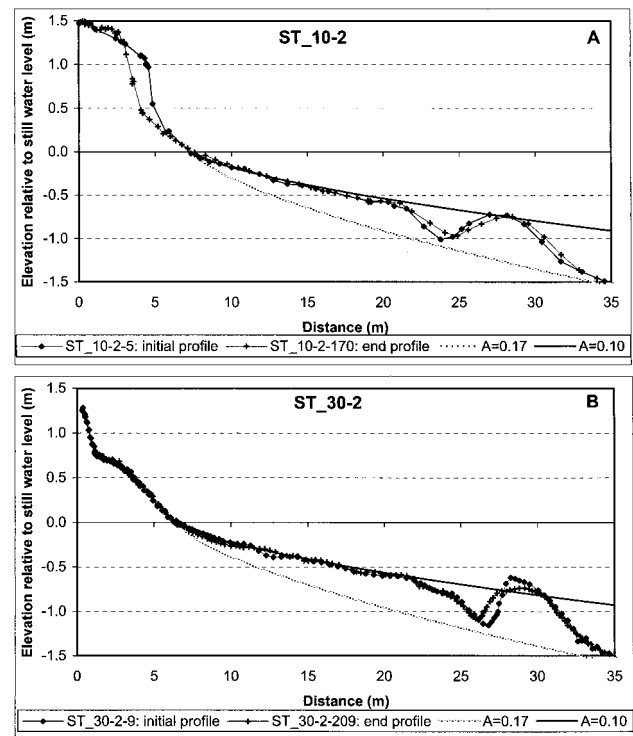


Figure 3. Initial and end beach profiles for ST.10-2 and ST.30-2, and the power-function profiles.

throughout the surf zone. The surf-zone profile was not as smooth, with several secondary bars (or large ripples) apparent, as compared to the profile during the irregular cases. The power-function model (Eq. 1) with $A = 0.17 \text{ m}^{1/3}$ over-predicts the water depth across most of the surf zone, whereas the lower $A = 0.10 \text{ m}^{1/3}$ under-predicts the water depth at most locations. The overall surf-zone profile is substantially different from that under irregular waves, although the regular wave case applied similar statistical significant wave height and peak wave period run in the irregular case.

For the accretory regular waves with smaller height (Figure 4B), substantial profile changes occurred after 559 min of wave action. The bar moved onshore substantially while preserving height. Slight advance of the shoreline occurred. The inner surf zone landward of the break-point bar gained a substantial amount of sand. Large bedforms, or secondary bars, developed on the seaward slope of the bar. The equilibrium profile shape with $A = 0.10 \text{ m}^{1/3}$ slightly over-predicts most of the profile except at the trough, whereas $A = 0.17 \text{ m}^{1/3}$ substantially over-predicts the water depth across nearly the entire profile.

The overall beach profile shape under regular waves was different as compared to the profile shape corresponding to the irregular waves of similar statistical significant wave height and peak period. The erosional regular wave produced a steeper profile, whereas the accretory regular wave resulted in a gentler profile. Also, secondary bars or large ripples developed in the mid-surf zone under regular waves, in

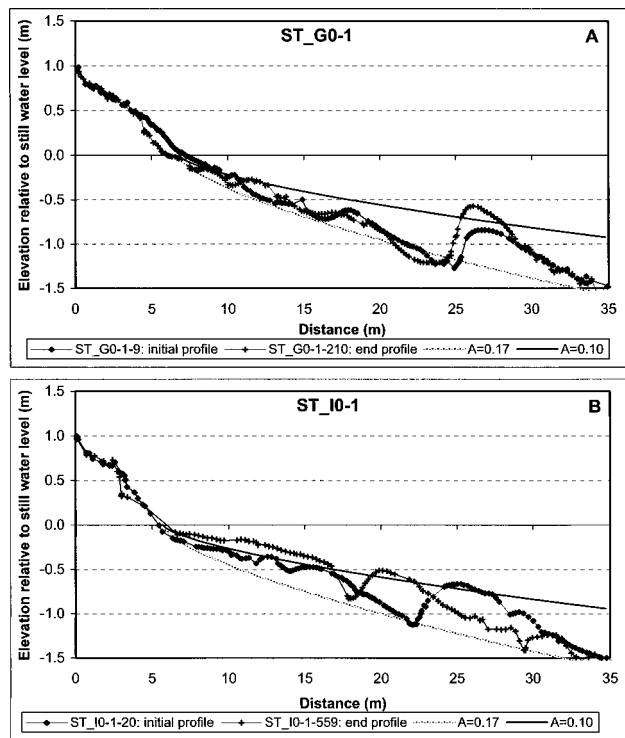


Figure 4. Initial and end beach profiles for ST_G0-1 and ST_I0-1, and the power-function profiles.

contrast to the smooth profile under irregular waves. The beach profile in the surf zone remained reasonably similar under irregular waves with different spectral characteristics, as well as statistical wave height and wave period. Constancy of profile shape supports present understanding that the *A*-value defining the equilibrium beach-profile shape is not significantly influenced by wave height, period, and spectral characteristics, leaving sediment grain size as the dominant factor controlling the beach-profile shape, as found in numerous previous studies using field data (e.g., DEAN, 1977; MOORE, 1982; MOUTZOURIS, 1991).

Patterns of Wave Decay and Breaker Index in the Surf Zone

In this study, the main breaker line for both regular and irregular wave cases was defined to be at the location landward of which a significantly steeper rate of wave-height decay was measured. This criterion was based on comprehension that substantial wave-energy loss or wave-height decrease should follow major wave breaking. The rate of wave decay at the breaker line may also provide information on the intensity of wave breaking. For example, WANG *et al.* (2002a) measured a much greater rate of wave-height decrease following plunging breaking than that following spilling breaking in a mid-scale laboratory facility.

Different patterns of wave decay were measured in ST_10-1 at the beginning and the end of the wave run (Figure 5A). At the breaker-point bar, a steeper decay in wave height oc-

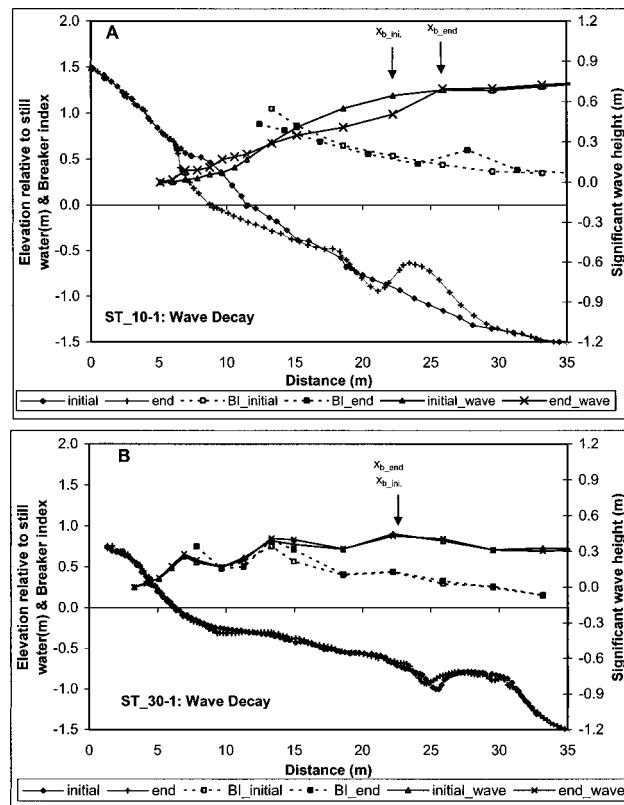


Figure 5. Cross-shore distributions of wave-height decay and breaker index over the initial and end beach profile for ST_10-1 and ST_30-1.

curring at the end of the wave run than at the beginning. This evolution in pattern of wave decay follows the evolution of the breakpoint bar and change in its seaward slope. SMITH and KRAUS (1991) showed that waves breaking on bars have different characteristics than those breaking on uniformly sloping beaches. In the vicinity of the shoreline, a gentler decay was measured at the end, probably influenced by the concave beach-profile shape there. Wave conditions seaward of the surf zone remained nearly identical during the 270 min wave action.

The breaker index (BI) $\gamma_{rms} = H_{rms}/h$ for irregular waves in the surf zone exhibited an increasing trend in value with distance from the breakpoint landward, from 0.37 at the breaker line to 1.05 in the swash zone at the beginning of the wave run (Figure 5A). At the end, a greater breaker-index value of 0.60 was measured at the breaker line, followed by a decrease landward to 0.45. Thereafter, a steady increasing trend to approximately 0.88 in the swash zone was measured, meaning that virtually all waves were breaking or had broken in that swash zone.

The patterns of wave decay at the beginning and end of the wave action for the other three irregular wave cases were nearly identical (Figure 5B; Figures 6A and B), especially for the two accretionary cases with relatively small wave heights (Figures 5B and 6B). Similar wave patterns are consistent with the stable beach profiles. The slight broadening and flat-

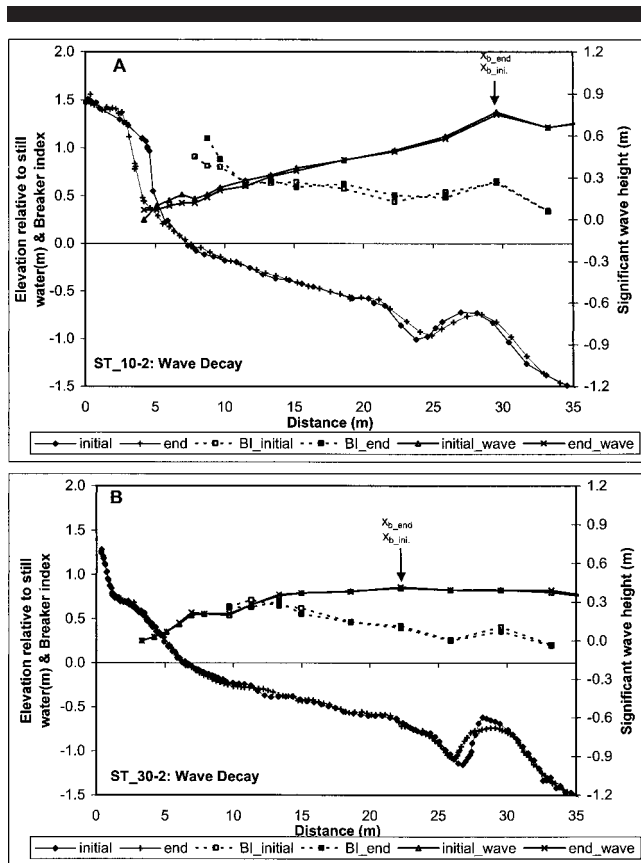


Figure 6. Cross-shore distributions of wave-height decay and breaker index over the initial and end beach profile for ST_10-2 and ST_30-2.

tening of the bar did not result in any substantial change in wave pattern over the bar. Breaking of the infrequent larger waves probably caused the slight flattening over the bar, which did not induce significant change in the overall wave height and wave-height decay over the bar.

The breaker index γ_{rms} increased from 0.20 over the seaward slope of the bar to 0.75 in the swash zone (Figures 5B and 6B). The decrease of H_{rms} and H_{sig} over the bar was not as steep as that in the higher wave cases (Figures 5A and 6A), indicating that wave breaking over the bar was not as significant. Steep wave decay, indicating major wave breaking, occurred close to the shoreline.

For the erosional wave case ST_10-2, the main breaker line as indicated by a steep decay of wave height was located over the bar crest (Figure 6A). At the beginning of the wave run, the wave decay in the vicinity of the shoreline was slightly gentler than that at the end of the run. The slight seaward movement of the bar during the 170 min wave action did not result in any distinguishable changes in the patterns of wave decay (Figure 6A).

The breaker index γ_{rms} exhibited similar cross-shore distribution pattern as that of ST_10-1, with a peak at the bar, followed by a moderate decrease, and then a landward increasing trend (Figure 6A). Over the bar, the breaker index

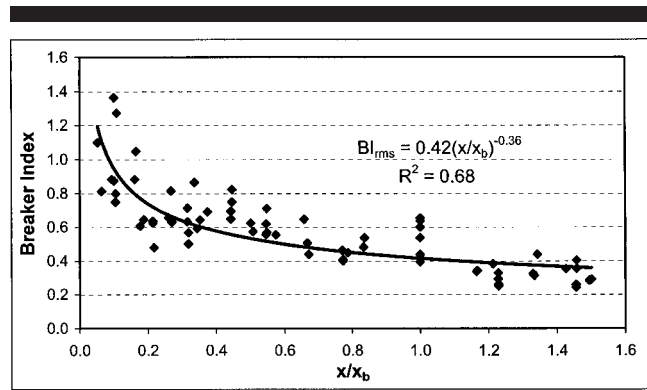


Figure 7. Cross-shore distribution of γ_{rms} .

equaled roughly 0.65, followed by a decrease to 0.44 over the trough, and then increased to 1.10 in the swash zone.

Overall, the breaker index γ_{rms} showed a landward increasing trend for all the four irregular wave cases. An increased γ_{rms} value over the breaker-point bar was produced by the combination of an increased wave height due to shoaling and the shallow water or the bar. Figure 7 compiles all γ_{rms} values for the four cases. The horizontal axis represents the dimensionless distance to the still-water shoreline, with x being the cross-shore distance to shoreline, and x_b is the width of the surf zone. This landward increasing trend of the breaker index across the surf zone is described reasonably well with a power function as:

$$\begin{aligned} \gamma_{rms} &= 0.416 \left(\frac{x}{x_b}\right)^{-0.36} \approx \gamma_{rms,b} \left(\frac{x}{x_b}\right)^{-1/3} \\ &= \gamma_{rms,b} \left(\frac{h}{h_b}\right)^{-2/9} \end{aligned} \quad (5)$$

where the term with the power -0.36 represents the least-square power-function fit of the measured γ_{rms} with the correlation coefficient R^2 equals 0.68. The right side of Equation (5) was obtained by substitution with Equation (1), and the representative value of $\gamma_{rms,b}$ fits well in the range of 0.42–0.44 reported by THORNTON and GUZA (1982, 1983) for field measurements.

Combining Equations (5) and (1), a simple equation for predicting the decay of H_{rms} across the surf zone of an equilibrium beach profile is obtained as

$$\begin{aligned} H_{rms} &= \gamma_{rms,b} A x^{1/3} x_b^{1/3} = \gamma_{rms,b} x_b^{1/3} \sqrt{A h} \\ &= \gamma_{rms,b} \sqrt{h_b h} \end{aligned} \quad (6)$$

where $\gamma_{rms,b}$ is the value of γ_{rms} at the point of incipient depth-limited wave breaking. The function at the second and third lines of the equation is obtained by substituting the power-function beach profile (Eq. 1) into the first line. Care should be exercised in determining $\gamma_{rms,b}$ over a barred profile and might best be defined past the plunge area of incipient breaking waves. For comparison, THORNTON and GUZA (1983) obtained the result $H_{rms} \sim h^{9/10}$ for irregular wave breaking on a plane sloping bottom as $h \rightarrow 0$ in the surf zone.

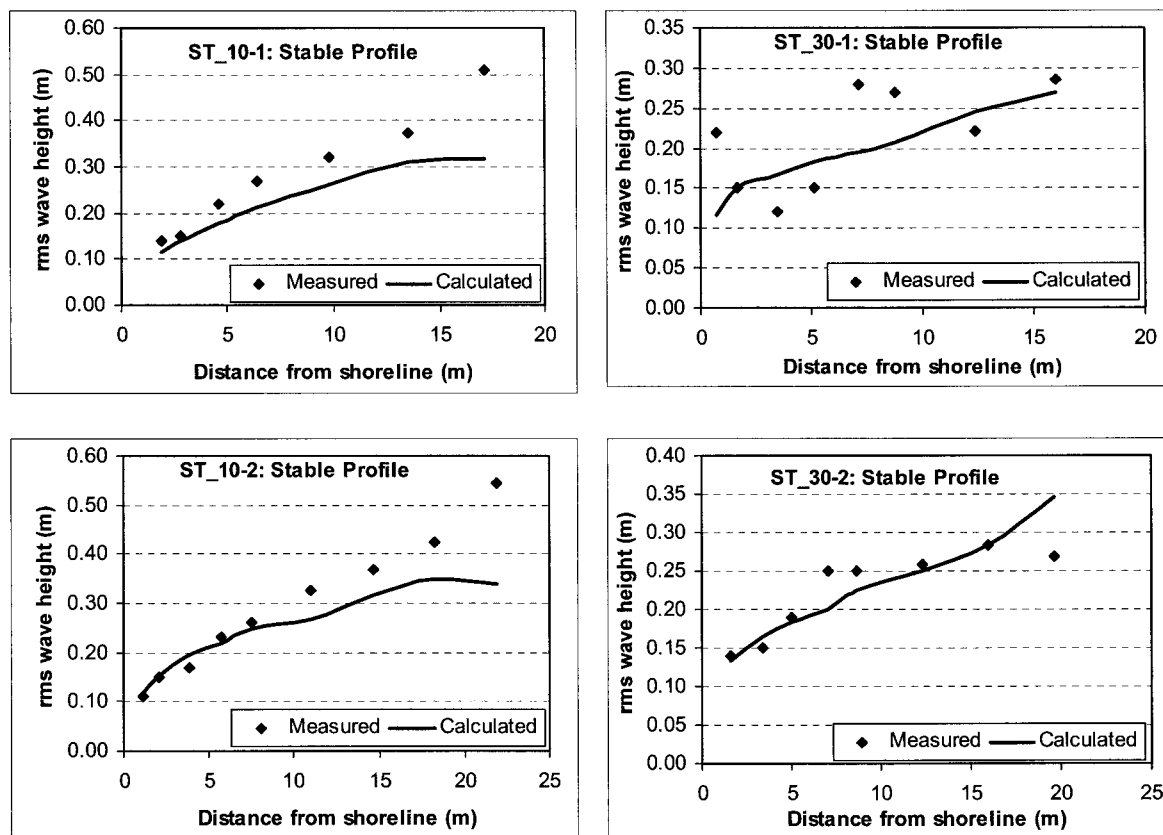


Figure 8. Measured and predicted (Eq. 6) wave heights across the surf zone, irregular wave cases.

Measured H_{rms} values were compared with the predicted ones from Equation (6). The surf-zone width x_b was measured from the still-water shoreline to the breaker line where relatively steep wave-energy dissipation occurred. The breaking depth h_b is determined based on Equation (1) from the measured x_b . The depth h_b can also be measured from the beach profile. However, measured h_b is not directly used here because it is sensitive to the relief of the bar. The best-fit $\gamma_{rms,b}$ value of 0.42 (Eq. 5) was used in the calculation. More data are necessary to improve the reliability and accuracy of a general $\gamma_{rms,b}$.

The H_{rms} was predicted reasonably well for the two erosional cases with higher waves (Figure 8: two left panels). The overall trend of wave decay was predicted well although the wave height was under-predicted at most locations except in the swash zone. A 10% increase in $\gamma_{rms,b}$ value would improve the match with the measured data. The wave height over the breaker-point bar was substantially under-predicted, and a discrepancy is expected because Equation (6) pertains to a monotonic beach profile.

For one of the two accretionary cases, ST_30-1 with narrow-peak wave and long period of 9 s, wave-height increases were measured at two locations, a short distance landward of the bar and directly seaward of the swash zone. These are likely due to wave reformation after breaking on the bar and shoaling before further breaking in the swash zone. Although

the complex variations of wave height were not predicted by Equation (6), the general trend was reproduced reasonably well (Figure 8: upper right panel). Equation (6) is developed based on the analysis of the monotonic equilibrium beach profile as given by Equation (1) and cannot reproduce complicated changes in wave height over a multiple bar profile.

Wave-height decay was reproduced well for the other random wave accretionary case, ST_30-2, except for over-prediction at the barred breaker-line (Figure 8: bottom right panel). Wave decay at the breaker line for the accretionary wave case with lower wave height was much gentler as compared to the erosional cases. The minor peak consisting of a reduced rate of wave decay followed by an increased rate in the mid-surf zone was not predicted.

The patterns of wave decay differed at the beginning and the end of the erosional regular wave case, ST_G0-1 (Figure 9A). At the beginning, a steady decrease in wave height with approach to shore was measured, whereas much steeper wave decay was measured over the bar after the 210 min wave action. The large wave-height decay from approximately 1.1 m to 0.4 m over the bar apparently resulted from the uniform breaking of regular waves over a narrow zone, in contrast to wider breaker zones of irregular waves. The wave height remained almost constant across most of the surf zone, followed by a steep decrease at the shoreline. Some wave-

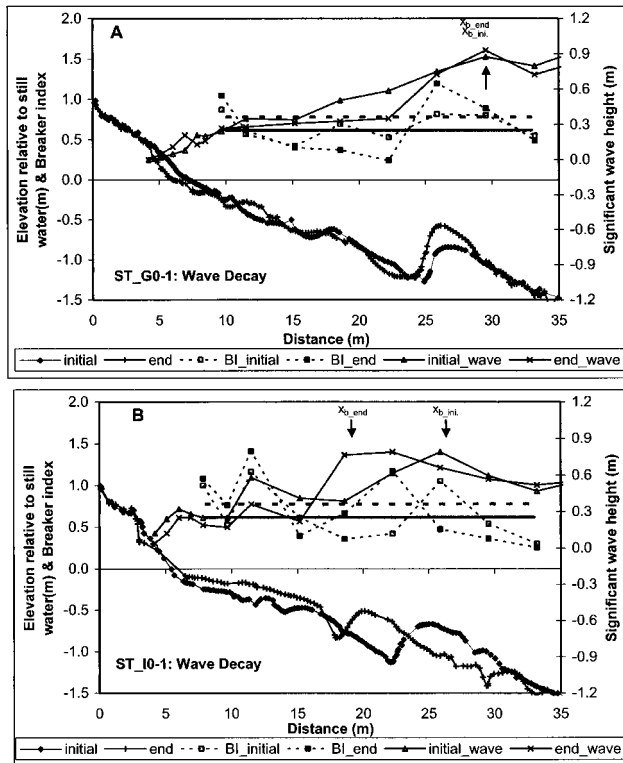


Figure 9. Cross-shore distributions of wave-height decay and breaker index over the initial and end beach profile for ST_G0-1 and ST_I0-1. The straight line represents $\gamma_{rms} = 0.62$ (solid line) and $\gamma = 0.78$ (dashed line).

height variations were measured seaward of the surf zone, probably resulting from formation of standing waves.

At the beginning of the wave run, the breaker index remained relatively uniform across shore, typically ranging from 0.53 to 0.87. At the end of the wave action, the value of the breaker index was nearly 1.20 at the breaker line, followed by a sharp drop to 0.24 over the trough and then a steady increase to approximately 1.04 in the swash zone. The standard $\gamma = 0.78$ found in regular wave studies (KAMINSKY and KRAUS, 1993) yielded over-predictions across most of the surf zone, except at the breaker line and in the swash zone (Figure 9A). Time-series wave analysis yielded an average H_{rms}/H_{sig} ratio of 0.80 in the surf zone for both of the two regular wave cases. This value is greater than the 0.71 obtained from the Rayleigh-distribution assumption. Outside the surf zone, the H_{rms}/H_{sig} ratio averaged 0.96, which is close to unity as expected for regular waves. A sharp decrease in the H_{rms}/H_{sig} ratio from nearly unity to approximately 0.8 occurred in the vicinity of the breaker line, or the narrow zone of initial wave breaking. The H_{rms}/H_{sig} ratio of 0.8 would yield a γ_{rms} value of 0.62 given the standard $\gamma_{sig} = 0.78$. The value $\gamma_{rms} = 0.62$, also plotted in Figure 9A, yielded an improved match with the measurements, with an average γ_{rms} value of 0.66.

Substantially different wave-decay patterns, as compared to the irregular wave cases, were also observed in the accre-

tionary regular wave case, ST_I0-1. The main breaker line as indicated by the steep wave-height decay moved onshore, consistent with the substantial onshore movement of the bar (Figure 9B). Somewhat regulated variations of the wave height, perhaps due to formation of partial standing waves, occurred both inside and outside the surf zone. The breaker index varied from 0.36 to over 1.41 across the surf zone. The landward increasing trend was not as steady as in the other cases. A breaker index greater than 1.0 was measured over the bar crest, *i.e.*, at the main breaker line, both at the beginning and at the end of the wave run. The standard $\gamma = 0.78$ matched the measured values (with an average of 0.74) better than the $\gamma_{rms} = 0.62$. The reason for this is not clear. Substantially different patterns and trends of wave-height decay were produced during regular-wave experiments, as compared to the results with irregular waves of similar statistical offshore significant wave height and peak period. The landward increasing trend of γ_{rms} during the regular wave cases was not as clear as that during the irregular wave cases. Equation (5) developed for irregular waves, does not describe the regular wave situation. A much greater value of γ_{rms} exceeding 1.0, was measured at the breaker line over the bar for the regular wave cases. As found from several previous regular wave studies (DALLY *et al.*, 1985; SMITH and KRAUS, 1987; SMITH and KRAUS, 1991), the wave-height-decay curve tends to be concave (curved or rounded downward). This is in contrast to the present irregular wave-decay curve, which has the sense of convex upward (somewhat rounded upward). The difference indicates that results obtained from simpler (in terms of wave generation) regular wave studies might not be directly applicable to irregular waves, similar to the situation of beach-profile change as discussed above. Wave irregularity should be considered in the modeling of wave-height decay and beach-profile evolution in the surf zone.

Patterns of Wave-Energy Dissipation Per Unit Volume

The key assumption of the DEAN (1977) equilibrium theory is that wave-energy dissipation per unit volume is uniform if the beach profile is in equilibrium. In the following, the assumption is examined with the SUPERTANK data.

Significantly different patterns of wave-energy dissipation per unit volume were measured at the beginning and end of ST_I0-1 (Figure 10A). At the beginning of the run, a substantial landward increasing trend was measured over the initial monotonic power-function profile. The wave-energy dissipation rate per unit volume increased from nearly zero just seaward of the surf zone to over 400 Nm/m³/s in the swash zone. After 270 min of wave action, the rate of wave-energy dissipation per unit volume became much more uniform, ranging from 54 to 155 Nm/m³/s with an average of 107 Nm/m³/s and a standard deviation of 43 Nm/m³/s. The equilibrium energy dissipation rate calculated from Equation (2) ($A = 0.1 \text{ m}^{1/3}$; $\gamma_{rms} = 0.56$) was 65 Nm/m³/s, approximately 39% lower than the average value of the measured dissipation rate. The value 0.56 for γ_{rms} was obtained by dividing the standard γ value of 0.78 (for significant wave height) by $\sqrt{2}$, on the assumption of a Rayleigh distribution in wave

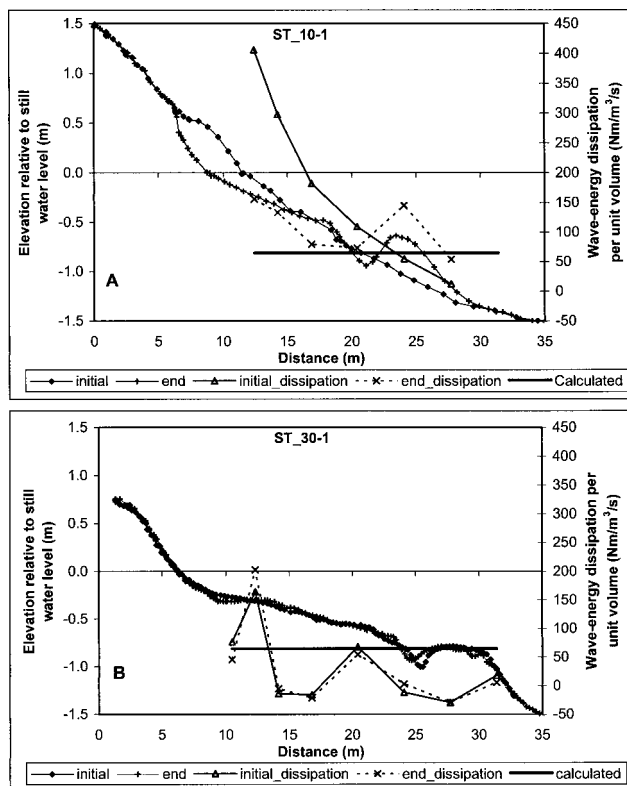


Figure 10. Wave-energy dissipation rate per unit volume over the initial and end beach profiles, and the computed equilibrium dissipation rate for ST.10-1 and ST.30-1.

height. At the end of the wave action, a high rate of wave-energy dissipation was measured over the bar crest at the main breaker line, followed by a sharp drop over the trough and a gradual increase toward the swash zone.

Although the measured γ_{rms} values were not uniform across the surf zone (as discussed in the previous section) and on average were greater than 0.56, they were not used in the Equation (2) calculation, because the equation was developed under the assumption of a constant γ under spilling breakers. Predictions from Equation (2) based on the simple equilibrium profile theory matched the measured values within 50% for this case.

Based on the overall beach-profile shape and the relatively minor profile changes in a series of following runs, it is reasonable to believe that the end profile after the 270 min of wave action should be close to the equilibrium shape. Large deviations from both measured and predicted equilibrium energy dissipation occurred near the shoreline and at the bar crest at the beginning of the ST.10-1 wave run. These deviations corresponded to substantial beach-profile change and, therefore, net cross-shore sediment transport. The results qualitatively support the transport equations (*e.g.*, Eq. 4) in the profile-change models of KRIEBEL and DEAN (1985) and LARSON and KRAUS (1989).

For the two irregular accretionary wave cases, the observed wave-energy dissipation was nearly the same at the begin-

ning and end of wave action (Figures 10B and 11B). This result implies nearly identical wave-decay pattern and beach-profile shape, indicating that the beach was already in near-equilibrium state at the beginning of the run. Due to the relatively small wave height, wave breaking over the bar crest may not be as significant as the high-wave cases, as also indicated by the small wave-energy dissipation rate at the bar crest. Major wave breaking occurred in a narrow zone near the shoreline, as indicated by increased dissipation of wave energy there. Overall, measured rates of wave-energy dissipation were moderately greater than the predictions from Equation (2) near the shoreline. In contrast, across the rest of the surf zone, the predicted rate was greater than the measured rates, which were only slightly above zero. Some wave regeneration was evident, particularly for ST.30-1 (the narrow-peaked swell type accretive wave case), as indicated by energy production (negative value of wave-energy dissipation). The 3.7-m spacing may also limit accuracy of calculation of energy dissipation where gradients in wave height are complicated or where waves are generated at the plunge point. On average, the wave-energy dissipation rate for the two accretionary cases was 46 $\text{Nm/m}^3/\text{s}$ for the narrow-peak swell-type waves and 44 $\text{Nm/m}^3/\text{s}$ for the broad-peak sea-type waves. The predicted value of 65 $\text{Nm/m}^3/\text{s}$ (Eq. 2) is 44% greater than the average measured value, although the measured values showed considerable variation across shore with a slight increasing trend toward the shoreline.

For the broadband erosional wave case, the patterns of wave-energy dissipation per unit volume were similar at the beginning and end of the wave action, ranging from 53 to 173 $\text{Nm/m}^3/\text{s}$ (Figure 11A). Little change in the beach profile occurred, indicating that it was probably near equilibrium at the beginning of the run. A great rate of wave-energy dissipation per unit volume was measured over the bar crest at the main breaker line, followed by a sharp decrease and a slight increase toward the swash zone. A sharp increase of the dissipation rate occurred in the swash zone. The wave-energy dissipation rate per unit volume across most of the mid-surf zone was relatively uniform and matched well with the value obtained from Equation (2). The two peaks in dissipation at the bar crest and in the swash zone were more than twice the predicted value from Equation (2).

Different patterns of wave-energy dissipation rate per unit volume were measured during the two regular wave cases, as compared to the irregular wave cases. Substantially different patterns were also measured at the beginning and the end of the wave run, consistent with the different beach-profile shapes and wave-height decay. At the beginning of the regular erosive wave case, the wave-energy dissipation rate per unit volume ranged from -43 to $402 \text{ Nm/m}^3/\text{s}$ with no apparent trend of changing. A negative wave-energy dissipation rate indicates an increase in wave height. This is apparent for the accretionary regular wave case. At the end of the 210 min wave action, a high dissipation rate of nearly $624 \text{ Nm/m}^3/\text{s}$ was obtained over the bar crest at the main breaker line, followed by a sharp decrease to $24 \text{ Nm/m}^3/\text{s}$ just landward of the trough (Figure 12A). The wave-energy dissipation rate remained close to zero across most of the mid-surf zone, and then increased to nearly $292 \text{ Nm/m}^3/\text{s}$ in the

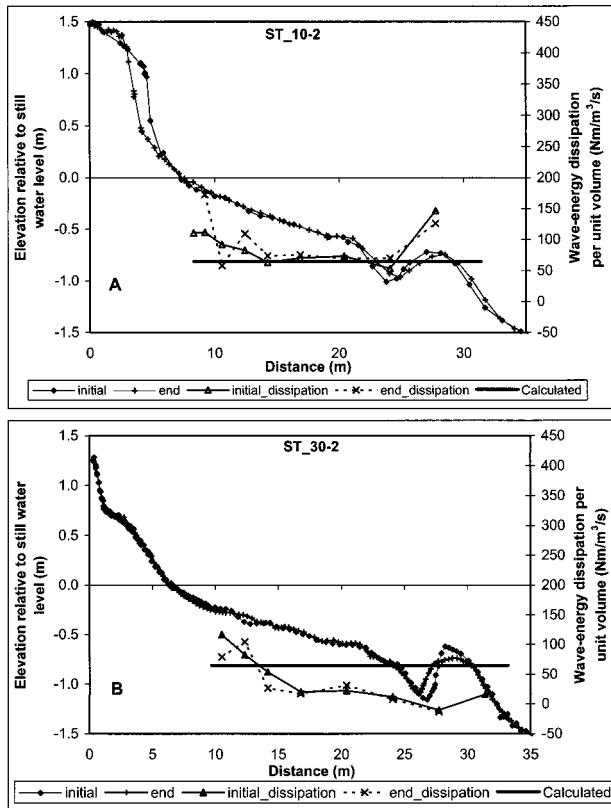


Figure 11. Wave-energy dissipation rate per unit volume over the initial and end beach profiles, and the computed equilibrium dissipation rate for ST-10-2 and ST-30-2.

swash zone. The pattern of wave-energy dissipation rate per unit volume deviated greatly from uniformity and differed significantly from the predicted value from Equation (2). Deviation from uniformity of wave-energy dissipation rate was much greater at the end of the wave run than at the beginning, influenced by the intense wave breaking over a narrow zone over the bar.

For the regular wave accretionary case, the energy dissipation rate per unit volume ranged from -204 to 637 $\text{Nm}/\text{m}^3/\text{s}$ at the beginning of the wave action, which is substantially different from the -296 to 751 $\text{Nm}/\text{m}^3/\text{s}$ at the end (Figure 12B). The dissipation patterns were far from being uniform and also differ substantially from the predicted value of 65 $\text{Nm}/\text{m}^3/\text{s}$.

The modulation of standing waves might have significant influence on the pattern of wave-energy dissipation for the regular wave cases, especially for the long-period accretionary wave case, as indicated by the large negative dissipation rate in the surf zone. The extremely high peak of wave-energy dissipation at the main breaker line in both of the regular wave cases is apparently related to the concentrated wave breaking over the bar.

The more gradual breaking of irregular as compared to regular waves tended to form a smoother beach profile and wave-decay pattern, whereas the localized breaking of regu-

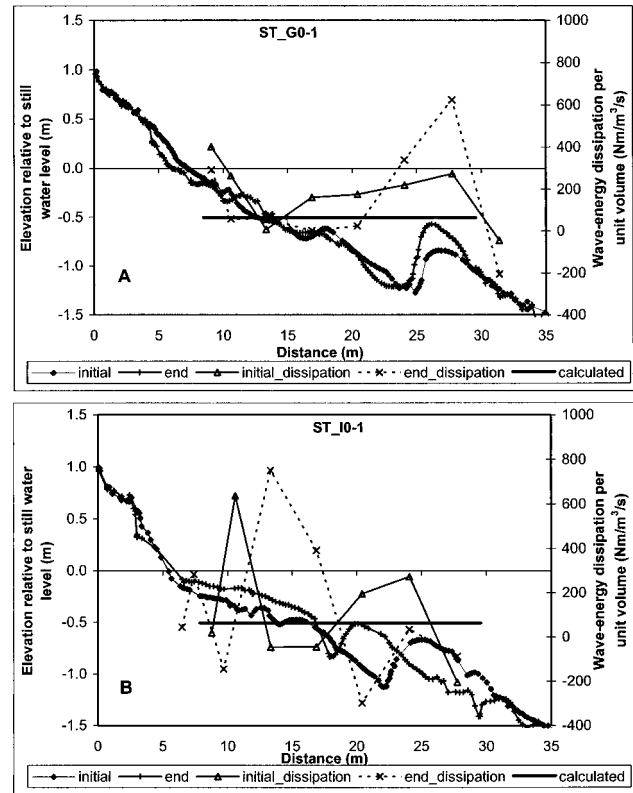


Figure 12. Wave-energy dissipation rate per unit volume over the initial and end beach profiles, and the computed equilibrium dissipation rate for ST-G0-1 and ST-I0-1.

lar waves produced more irregularity in the beach profile and shape of wave decay. Given the steadiness of the monochromatic waves, concentrated wave breaking and energy dissipation should be expected, especially for plunging type breaking. The deviation of H_{rms}/H_{sig} from unity in the surf zone for regular waves indicates a certain amount of wave irregularity is generated in the breaking process. No substantial differences were found between the narrow-banded swell-type waves and broad-banded sea-type waves in the data examined in this study.

CONCLUSIONS

In the six SUPERTANK cases analyzed, a nearshore bar developed and was maintained over an initially monotonic power-function profile. Except in the direct vicinity of the break-point bar, the power-function model of DEAN (1977) described the equilibrium beach profile reasonably well. For irregular waves, the assumption that an equilibrium profile shape develops under uniform wave-energy-flux dissipation is supported by the SUPERTANK data across a large portion of the surf zone. Relatively greater rates of wave-energy dissipation were measured at the main breaker line and in the swash zone. The equilibrium rate of wave-energy dissipation was predicted mostly within 50% by the simple model derived by DEAN (1977) with a spilling breaking assumption. Signif-

icant net cross-shore sediment transport and beach-profile change occurred at locations where the rate of wave-energy dissipation deviated substantially from the equilibrium rate.

For irregular waves, in the surf zone the root-mean-square wave height on an equilibrium beach profile was found to be proportional to the square root of local water depth, except over the break-point bar. The more gradual wave-height decay contrasts to the common spilling wave breaker assumption for which the wave height is proportional to local water depth in the surf zone. The simple model, requiring the input of the equilibrium A value and the bounds of the surf zone, reproduced the measured wave decay reasonably well under different large-scale laboratory wave and beach conditions.

Both beach-profile evolution and wave-energy dissipation pattern differ substantially under regular waves as compared to those under irregular waves of comparable statistical significant wave height and peak period. Different beach profile shapes were developed under regular waves, particularly in the vicinity of the break-point bar. For the regular wave cases, uniformity of wave-energy dissipation did not improve between the start and end of wave actions. These results indicate studies with regular waves may not represent all sediment-transport processes as associated with irregular waves. A key difference is that wave-energy dissipation for regular waves tends to be concentrated in a narrow zone of breaking. Knowledge of cross-shore sediment transport gained from regular-wave experiments will carry uncertainties if applied to irregular waves without appropriate interpretation or treatment of the regular waves, such as through a Monte Carlo approach.

For the irregular wave cases analyzed, there were relatively small differences between breaker index values, wave decay, and energy-dissipation rate per unit volume for the broad and narrow-banded waves. This result, based on limited laboratory data but at large scale, indicates that the influences of spectral characteristics of irregular waves on the beach-profile evolution are not significant for typical waves with single-peaked spectra.

ACKNOWLEDGMENTS

The work of P. Wang was jointly funded by the Coastal Inlets Research Program (CIRP) administered at the U.S. Army Engineer Research and Development Center and by the Louisiana Sea Grant College Program. The work of N.C. Kraus was conducted under the Inlet Geomorphology and Channel Evolution work unit of the CIRP. We appreciate critical reviews and helpful comments by Drs. Magnus Larson and Jane McKee Smith. Permission was granted by Headquarters, U.S. Army Corps of Engineers to publish this paper.

LITERATURE CITED

- BOUWS, E.H.; ROSENTHAL, G.W., and VINCENT, C.L., 1985. Similarity of the wind wave spectral in finite water depth, 1: spectral form. *Journal of Geophysical Research*, 90, 975–986.
- BRUN, P., 1954. Coast erosion and the development of beach profiles. *Technical Memorandum No. 44*, Beach Erosion Board, U.S. Army Corps of Engineers.
- DALLY, W.R.; DEAN, R.G., and DALRYMPLE, R.A., 1985. Wave height variation across beaches of arbitrary profile. *Journal of Geophysical Research*, 90, 11,917–11,927.
- DEAN, R.G., 1977. Equilibrium beach profiles: U.S. Atlantic and Gulf coasts. *Ocean Engineering Report No. 12*, Department of Civil Engineering, University of Delaware, Newark, DE.
- DEAN, R.G., 1991. Equilibrium beach profiles: characteristics and applications. *Journal of Coastal Research*, 7, 53–84.
- GONZALEZ, M.; MEDINA, R., and LOSADA, M.S., 1999. Equilibrium beach profile model for perched beaches. *Coastal Engineering*, 36, 343–357.
- INMAN, D.L.; ELWANY, M.H.S., and JENKINS, S.A., 1993. Shore rise and bar-berm profiles on ocean beaches. *Journal of Geophysical Research*, 98(C10), 18,181–18,199.
- KAMINSKY, G.M. and KRAUS, N.C., 1993. Evaluation of depth-limited wave breaking criteria. *Proceedings of 2nd International Symposium on Ocean Wave Measurement and Analysis, Waves 93* (ASCE, New York), pp. 180–193.
- KRAUS, N.C.; LARSON, M., and KRIEBEL, D.L., 1991. Evaluation of beach erosion and accretion predictors. *Proceedings Coastal Sediments '91* (ASCE, New York), pp. 572–587.
- KRAUS, N.C. and SMITH, J.M., 1994. SUPERTANK laboratory data collection project, Volume 1: Main text. *Technical Report CERC-94-3*, U.S. Army Engineer Waterways Experiment Station, Coastal Engineering Research Center, Vicksburg, Mississippi.
- KRAUS, N.C.; SMITH, J.M., and SOLLITT, C.K., 1992. SUPERTANK Laboratory Data Collection Project. *Proceedings 23rd Coastal Engineering Conference* (ASCE, New York), pp. 2191–2204.
- KRAUS, N.C. and LARSON, M., 1988. Prediction of initial profile adjustment of nourished beaches to wave action. *Proceedings of 1988 National Conference on Beach Preservation Technology*, Florida Shore and Beach Preservation Association, Tallahassee, Florida, pp.125–137.
- KRIEBEL, D.L., 1986. Verification study of a dune erosion model. *Shore and Beach*, 54(3), 13–21.
- KRIEBEL, D.L. and DEAN, R.G., 1985. Numerical simulation of time-dependent beach and dune erosion. *Coastal Engineering*, 9, 221–245.
- KRIEBEL, D.L. and SMITH, J.M., 1994. Wave transformation measurements at SUPERTANK. *Proceedings Coastal Dynamics '94* (ASCE, New York), pp. 223–247.
- LARSON, M., 1991. Equilibrium profile of a beach with varying grain size. *Proceedings Coastal Sediments '91* (ASCE, New York), pp. 861–874.
- LARSON, M. and KRAUS, N.C., 1989. SBEACH: Numerical modeling for simulating storm-induced beach change—Report 1: empirical foundation and model development. *Technical Report, CERC-89-9*, U.S. Army Engineer Waterways Experiment Station, Coastal Engineering Research Center, Vicksburg, Mississippi.
- LARSON, M. and KRAUS, N.C., 1994a. Temporal and spatial scales of beach profile change, Duck, North Carolina. *Marine Geology*, 117, 75–94.
- LARSON, M. and KRAUS, N.C., 1994b. Cross-shore sand transport under random waves at SUPERTANK examined at mesoscale. *Proceedings Coastal Dynamics '94* (ASCE, New York), pp. 204–219.
- LARSON, M. and KRAUS, N.C., 2000. Representation of non-erodible (hard) bottoms in beach profile change modeling. *Journal of Coastal Research*, 16(1), 1–14.
- LARSON, M.; KRAUS, N.C., and WISE, R.A., 1999. Equilibrium beach profiles under breaking and non-breaking waves. *Coastal Engineering*, 36, 59–85.
- MCDUGAL, W.G.; KRAUS, N.C., and AJTWIBOWO, H., 1996. The effects of seawalls on the beach: Part II, numerical modeling of SUPERTANK seawall tests. *Journal of Coastal Research*, 12(3), 702–713.
- MOORE, B.D., 1982. Beach profile evolution in response to changes in water level and wave height, *Masters Thesis*, Department of Civil Engineering, University of Delaware, Newark, Delaware.
- MOUTZOURIS, C.I., 1991. Beach profile vs. cross-shore distribution of sediment grain size. *Proceedings of Coastal Sediments '91* (ASCE, New York), pp. 419–431.
- PRUSZAK, Z., 1993. The analysis of beach profile changes using Dean's method and empirical orthogonal functions. *Coastal Engineering*, 19, 245–261.

- SMITH, J.M., 1994. Undertow at SUPERTANK. *Proceedings Coastal Dynamics '94* (ASCE, New York), pp. 220–232.
- SMITH, E.R. and KRAUS, N.C., 1991. Laboratory study of breaking waves on bars and artificial reefs. *Journal of Waterway, Port, Coastal and Ocean Engineering*, 117(4), 307–325.
- SMITH, J.M. and KRAUS, N.C., 1987. Longshore current model based on power law wave decay. *Proceedings Coastal Hydrodynamics '87* (ASCE, New York), pp. 155–169.
- SMITH, J.M. and KRAUS, N.C. (Editors), 1995. SUPERTANK laboratory data collection project, Volume II: Appendices A-I. *Technical Report CERC-94-3*, U.S. Army Engineer Waterways Experiment Station, Coastal Engineering Research Center, Vicksburg, Mississippi.
- THORNTON, E.B. and GUZA, R.T., 1982. Energy saturation and phase speeds measured on a natural beach. *Journal of Geophysical Research*, 84, 9,499–9,508.
- THORNTON, E.B. and GUZA, R.T., 1983. Transformation of wave height distribution. *Journal of Geophysical Research*, 88, 5,295–5,938.
- WANG, P. and DAVIS, R.A., 1998. A beach profile model for a barred coast—case study from Sand Key, West-Central Florida. *Journal of Coastal Research*, 14, 981–991.
- WANG, P. and DAVIS, R.A., 1999. Depth of closure and the equilibrium beach profile—A case study from Sand Key, West-Central Florida. *Shore and Beach*, 67, 33–42.
- WANG, P.; SMITH, E.R. and EBERSOLE, B.A., 2002a. Large-scale laboratory measurements of longshore sediment transport under spilling and plunging breakers. *Journal of Coastal Research*, 18, 118–135.
- WANG, P.; EBERSOLE, B.A.; SMITH, E.R., and JOHNSON, B.D. 2002b. Temporal and spatial variations of surf-zone currents and suspended-sediment concentration. *Coastal Engineering*, 46, 175–211.
- WORK, P.A. and DEAN, R.G., 1991. Effect of varying sediment size on equilibrium beach profiles. *Proceedings of Coastal Sediments '91* (ASCE, New York), pp. 891–903.
- ZHENG, J. and DEAN, R.G., 1997. Numerical models and intercomparisons of beach profile evolution. *Coastal Engineering*, 30(3–4), 169–201.